16th World Conference on Earthquake, 16WCEE 2017
Santiago Chile, January 9th to 13th 2017
Paper N° 2201
Registration Code: S-I1461879556

STUDY ON POUNDING EFFECT BETWEEN SHORT-TO-MID HEIGHT RC BUILDINGS WITH ALIGNED SLABS

A. Kharazian(1), F. López-Almansa(2)
(1) PhD. Candidate, Technical University of Catalonia, alireza.kharazian@upc.edu
(2) Professor, Technical University of Catalonia, francesc.lopez-almansa@upc.edu

Abstract

This work presents a parametrical numerical study of pounding between short-to-mid height RC framed buildings with aligned slabs. The study consists in analyzing the dynamic response of four 3 and 5-storey prototype colliding buildings to four representative accelerograms.

Keywords: Pounding; RC buildings; Nonlinear Analysis

1. Introduction

Pounding between adjoining buildings during strong seismic events is a serious problem, been proven highly damaging in past earthquakes [1]. This paper describes a parametrical numerical study on the consequences of pounding between adjoining short-to-mid height RC framed buildings with aligned slabs. The study consists in analyzing the dynamic response of colliding buildings to a number of representative strong seismic inputs.

Four 3 and 5-story buildings with 2 and 5 bays are selected for this work. To represent the most common situations, the structural configuration of the selected buildings has plan symmetry and uniformity along height. Buildings are designed for a high seismicity region following international (American-based) regulations. Structure consists of square columns, rectangular deep beams, and flat slabs; contribution of other members, such as infill walls, is not considered.

Nonlinear behavior of buildings is simulated with frame finite element models; nonlinearities are concentrated in plastic hinges located at ends of each element (concentrated plasticity). Moment-curvature laws are obtained from fiber models. Nonlinear concrete behavior is represented by a constant-confinement model; confinement effect is described by an effective confinement stress which depends on longitudinal and transverse reinforcement. Tensile concrete strength is neglected. Steel behavior is described by uniaxial bilinear constitutive laws with kinematic strain hardening; hardening rule for yield surface is a linear function of increment of plastic strain. Time integration is carried out using Newmark algorithm. Particular attention has been paid to time step selection, given that pounding generates sudden changes in extremely short time intervals, thus leading to important accelerations and involving higher modes response. Pounding is described by a Kelvin-Voigt linear gap model. Despite this model is termed as linear, it is actually nonlinear, since gap behaves as a “compression only” element. In the gap model, spring stiffness is selected proportional to axial stiffness of colliding slabs and damping factor is chosen to provide a desired restitution factor; gap size is chosen to represent actual situations. Soil-Structure Interaction (SSI) is described differently for foundations with spread footings and mats. In both cases, SSI is simulated by parallel combination of elastic springs and dashpots linking foundation and underlying soil. All these models are jointly implemented in SeismoStruct software package.

Four representative recorded inputs are selected; are obtained combining presence or absence of velocity pulses, and stiff / soft soil conditions. Three accelerograms correspond to Northridge earthquake (January 17, 1994) and the fourth one belongs to Victoria earthquake (Mexico, June 9, 1980). Acceleration and energy response spectra are generated to highlight inputs characteristics.

The parameters of the study are those of the selected buildings, the inputs (including soil conditions), the gap model, and the SSI. Effects of pounding are evaluated through four performance indices:

- Maximum drift angle. Provides, for each story, information on damage on beams and columns and on infill walls.
- Maximum shear force. Reports also on structural damage. In first floor, is base shear force; it provides information on demanding on foundation.
- Hysteretic energy. Absorbed energy minus energy absorbed by initial structural damping. Reports on damage in terms of cumulated values.
- Maximum absolute acceleration. Provides information on damage to non-structural components.

The preliminary results show regular and expected behavior. This corroborates the accuracy and reliability of the used model.

2. Prototype buildings

2.1 General considerations

Prototype buildings have been selected aiming to its representativeness, mainly in developing countries (where pounding is more feasible). Noticeably, main objective of this research is to analyze pounding between pairs of buildings, not to study the behavior of single buildings; therefore, representativeness should be placed within this context. Buildings are assumed to be provided with adequate seismic design for high seismicity regions; conversely, gap is insufficient. This situation is frequent in developing countries, since commonly design fulfils all legal requirements (to obtain construction permits) but construction control is not completely strict. Most of the actual buildings have plan symmetry and asymmetric plan layouts are difficult to categorize. Regarding uniformity along height, situation is similar; therefore, only symmetric and regular buildings are considered. This regularity implies that columns are uniformly distributed, and are no interrupted (continuous down to foundation), and that story height is constant. Cooperation of the masonry infill walls is not taken into consideration because lack of reliability and because frequently walls are separated from main frame to allow for relative motion. Since vast majority of buildings in developing countries have only moderate height, only short to mid-height buildings are considered. Regarding use, most of buildings are intended for housing and administrative use; other close uses (commercial, schools, sanitary facilities, among others) are also possible.

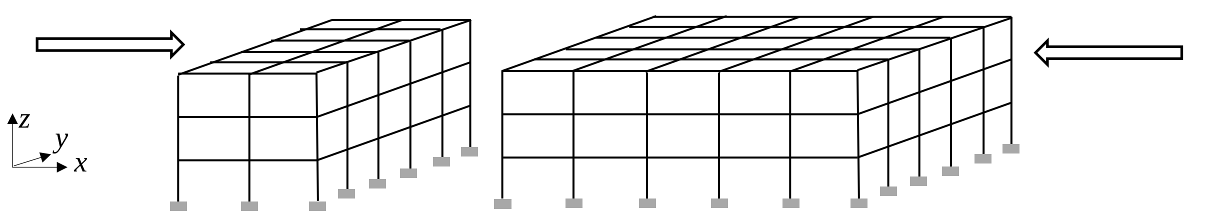

(a) Three-story two-bay building (3 × 2) (b) Three-story five-bay building (3 × 5)

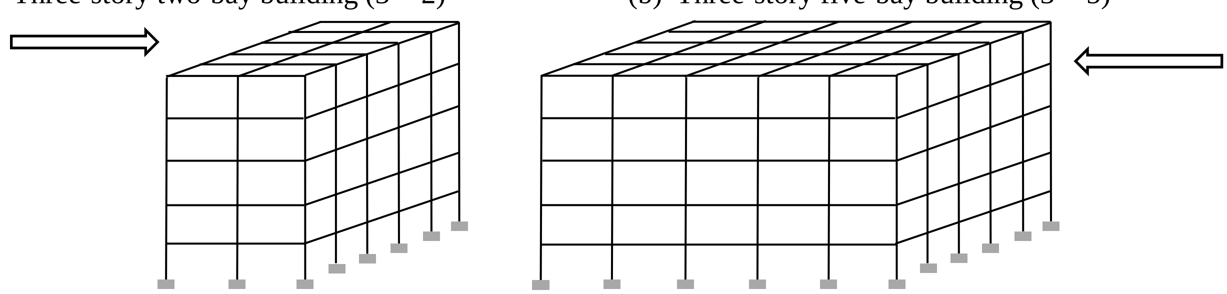

(c) Five-story two-bay building (5 × 2) (d) Five-story five-bay building (5 × 5)

Fig. 1 – Prototype buildings

2.2 Description of the prototype buildings

Four housing or administrative prototype buildings have been selected to represent the most common situations. All buildings have RC framed structure with square columns, two-way solid slabs and rectangular cast-in-situ beams joining the columns, see Fig. 1.

As shown in Fig. 1, the buildings have uniformity in elevation and symmetry in plan, with rectangular plan layout. There are no basements. There are six frames (five bays) in direction parallel to the joint between the colliding buildings (y); in the other direction (x) the number of bays of each building ranges in between two and five to account for the differences in mass among both buildings. Along this study, N represents the number of stories and b is the number of bays in direction orthogonal to the joint between the buildings (x, Fig. 1); every building is denoted by $N \times b$. The story height is 3.2 m and the span length is 5 m in both directions. The beams section is 40×50 cm^2 and the slabs are 15 cm deep. Inside each story, all the columns are alike, even the reinforcement; Table 1 depicts the cross sections of the columns.

Table 1 – Representative buildings

Building	**Height (m)**	**1st floor columns (cm)**	**2nd floor columns (cm)**	**3rd floor columns (cm)**	**4th floor columns (cm)**	**5th floor columns (cm)**	**Fundamental periods (s)**	**Weight (kN)**
3 × 5	9.6	60 × 60	55 × 55	50 × 50	-	-	0.259	3709
3 × 2	9.6	60 × 60	55 × 55	50 × 50	-	-	0.247	1526
5 × 5	16	60 × 60	55 × 55	50 × 50	45 × 45	40 × 40	0.464	6067
5 × 2	16	60 × 60	55 × 55	50 × 50	45 × 45	40 × 40	0.444	2486

The characteristic values of the concrete compressive strength and of the steel yielding point are f'_c = 30 MPa and f_y = 500 MPa, respectively. The buildings are designed according to the ACI and ASCE codes [2, 3]. Dead loads: self-weight + flooring + partitioning = 8 kN/m^2, roof self-weight + flooring + partitioning = 6.8 kN/m^2, cladding 3/2.6 kN/m^2. Live loads: floors 2 kN/m^2, roof 1.5 kN/m^2, stairs 3.5 kN/m^2. The loading combination is 1.2 D + 1.6 L. The seismic design is performed for 0.4 g design acceleration, corresponding to 475 years return period (10% probability of being exceeded in 50 years). The soil can be either stiff or soft, with shear wave velocity in between 360 and 800 m/s or 180 and 360 m/s, respectively; they correspond to types C and D according to ASCE classification [3] and to types B and C according to the EC-8 classification [4]. Given that softer soil leads to more demanding forces, it has been considered for design. For design purposes, the structure of the buildings is modelled as a 3D frame of beams and columns with rigid connections among them; the columns are assumed to be clamped to the foundation. The beams are modelled as T-section members; the effective width is 105 cm for the inner beams and 70 cm for the side beams [2]. The concrete cracking is taken into account by reducing the moments of inertia of beams and columns by factors 0.40 and 0.7, respectively [5]. The contribution of the staircases, infill walls and other elements to the lateral resistance of the building is neglected. The seismic design is carried out through equivalent static analysis. For serviceability conditions, the drift limit is 0.02 H for the 3-storey building and 0.025 H for the 5-storey building. The fundamental periods of the buildings are estimated from the empirical expressions contained in the ASCE code; for the 3 and 5-storey buildings it is initially assumed that T_F = 0.3 s and 0.5 s, respectively. The assumed damping factor is 5%. The buildings are considered of normal importance (Risk Category II), therefore, seismic importance factor is I_e = 1. The response reduction factor is 5, corresponding to "intermediate reinforced concrete moment frames" according to the ASCE code. The contributing mass of the slab is uniformly distributed among all the frames. The site seismicity for 4975 years return period (1% probability of being exceeded in 50 years) corresponds to coefficients S_S = 2.098 g, S_1 = 0.994 g (spectral response acceleration parameters), F_a = 1, F_v = 1.5 (site coefficients based on and S_S and on S_1, respectively). In the design spectrum the left and right abscissae of the plateau are T_0 = 0.142 s and T_S = 0.711 s, respectively. Assumed risk category and seismicity determine Seismic Design Category D. Noticeably, 3-story buildings are designed as if they were 5-story; it means that demanding forces on members are determined as if buildings had five stories.

The fundamental periods are obtained by classic linear eigenvalue analysis by discretizing the buildings by classical lumped masses models. As discussed next, buildings are merely represented by single 2-D frames;

accordingly, Table 2 displays the masses of each story (including the corresponding masses of columns and other vertical elements) for the lone buildings. Figures from Table 2 correspond to D + 0.2 L.

Table 2 – Mass (kg) of each frame of the individual buildings

Story No.	**Building**			
	3 × 5	**3 × 2**	**5 × 5**	**5 × 2**
1	127239	52452	127239	52452
2	124762	51214	124762	51214
3	117598	47632	122392	50029
4	-	-	120180	48923
5	-	-	115386	46526

Table 3 displays natural periods and modal mass ratios of the individual buildings. Given that pounding is described as a 2-D phenomenon, only translational modes in x direction are considered. Table 3 shows regular behavior, with well-separated periods and clear predominance of first mode.

Table 3 – Natural periods (s) and modal mass ratios of the individual buildings

Mode No.	**Building**							
	3 × 5		**3 × 2**		**5 × 5**		**5 × 2**	
	T	m_i^* / m	T	m_i^* / m	T	m_i^* / m	T	m_i^* / m
1	0.259	0.8327	0.247	0.8276	0.464	0.7633	0.444	0.7618
2	0.091	0.1186	0.085	0.1219	0.179	0.1289	0.167	0.1295
3	0.054	0.0486	0.050	0.0504	0.109	0.0499	0.101	0.0500
4	-	-	-	-	0.077	0.0313	0.071	0.0314
5	-	-	-	-	0.054	0.0265	0.049	0.0271

2.3 Foundation

Since there are no basements, soil quality is assumed to be good, and buildings height is rather moderate, foundation is assumed to be shallow (direct). Given that soil type can be either soft or stiff and that there is no direct correlation between soil type and bearing capacity, it is necessary to assume several levels of soil strength. Two levels are considered: poor soil (bearing capacity 0.15 MPa) and good soil (allowable stress 0.4 MPa). For strong soil, foundation consists in isolated (pad or spread) footings connected with ties. Ties are intended to avoid horizontal relative displacements between footings, i.e. influence of spatial variation of seismic action. As well, ties will provide recentering effect on pads; this being particularly convenient for eccentric footings. This layout will prevent completely the risk of local uplift at some footings. Each footing (except eccentric ones) is 3 m × 3 m × 1.5 m. Structural parameters (concrete and steel strength and reinforcement amount) are not detailed herein because are not relevant to the objectives of this work. For poor soil, mat (slab) foundation is considered, since, with isolated footings, digging would affect more than half of building plan, thus making this solution impractical. Slab depth is 1 m. As in the isolated footings solution, structural parameters are not detailed.

2.4 Structural modelling of the prototype buildings

Pounding is described as a 2-D phenomenon, without accounting for torsion effects. Therefore, buildings are merely represented by single 2-D frames. Given that all parallel frames are alike (Fig. 1), this assumption describes adequately pounding between buildings provided that one sixth of building mass is assigned to each frame (Table 2).

The nonlinear dynamic structural behavior of the frames is described with 2-node frame finite element models (Fig. 2.a); each member (e.g. beam or column) is represented by a single element. Nonlinearities are concentrated in plastic hinges located at the ends of each element (concentrated plasticity, Fig. 2.b). This choice relies reduced analysis time and avoid localization issues, e.g. dependency on the number of Gauss points [6, 7]. The moment-curvature behavior of each hinge is depicted by fiber models SeismoStruct [6] with 300 fibers in each section. The length of the hinges is established according the well-known empirical criterion proposed in [8].

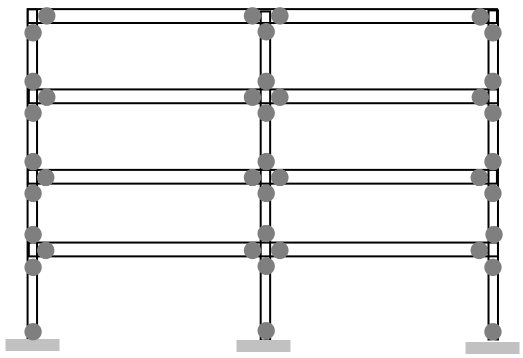

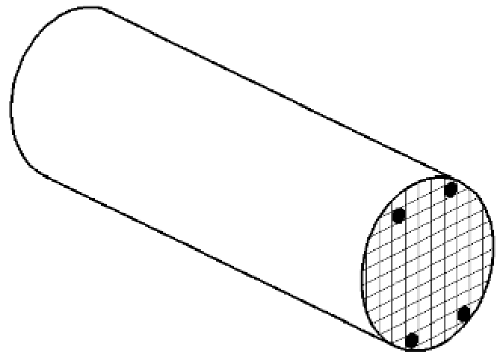

(a) Frame discretization and plastic hinge locations

(b) Fibre model

Fig. 2 – Finite element modelling

The nonlinear behavior of the concrete is represented by a constant-confinement concrete model [9, 10, 11]; the confinement effect is described by an effective confinement stress which depends on the longitudinal and transverse reinforcement. This model proposes a unified stress-strain approach for confined concrete for both circular and rectangular transverse reinforcement:

$$\sigma_c = \frac{f'_{cc}\, x\, r}{r - 1 + x^r} \tag{1}$$

In Eq. (1), σ_c is concrete stress and f'_{cc} is compressive strength of confined concrete. Coefficient $x = \frac{\varepsilon_c}{\varepsilon_{cc}}$, where ε_c is concrete strain and ε_{cc} is strain at peak stress related to f'_{cc}: $\varepsilon_{cc} = \varepsilon_{c0}\left[1 + 5\left(\frac{f'_{cc}}{f'_{c0}} - 1\right)\right]$; in this expression, ε_{c0} and f'_{c0} are strain and unconfined concrete strength, respectively. Coefficient $r = \frac{E_c}{E_c - E_{sec}}$, where E_c and E_{sec} are the initial and secant concrete deformation modulus; $E_{sec} = \frac{f'_{cc}}{\varepsilon_{cc}}$.

It can be shown [9] that the confined compressive strength is related to the unconfined one by $f'_{cc} = f'_{c0}\, K$, where K is a confinement factor given by:

$$K = -1.254 + 2.254\sqrt{1 + \frac{7.94 f'_l}{f'_{c0}}} - 2\frac{\sigma'_l}{f'_{c0}} \tag{2}$$

In Eq. (2), σ'_l is effective lateral confining pressure given by $\sigma'_l = k_e \sigma_l$ where k_e and σ_l are confinement effectiveness coefficient and lateral confining pressure, respectively. Confinement coefficient is defined as ratio $k_e = \frac{A_e}{A_{cc}}$, where $A_e = (b_c d_c - A_i)\left(1 - \frac{s'}{2\, b_c}\right)\left(1 - \frac{s'}{2\, d_c}\right)$ and $A_{cc} = b_c d_c - A_{st}$. In these expressions, b_c and d_c are core dimensions of confined (rectangular) area, *s'* is clear separation between consecutive transverse reinforcement bars, A_{st} is longitudinal reinforcement area, and $A_i = \sum_{i=1}^{n}\left(\frac{w_i^2}{6}\right)$ where w_i represents clear separation between consecutive tied longitudinal reinforcement bars and *n* is the number of such bars. Fig. 3 illustrates the meaning of geometrical parameters b_c, d_c, *s'*, and w_i.

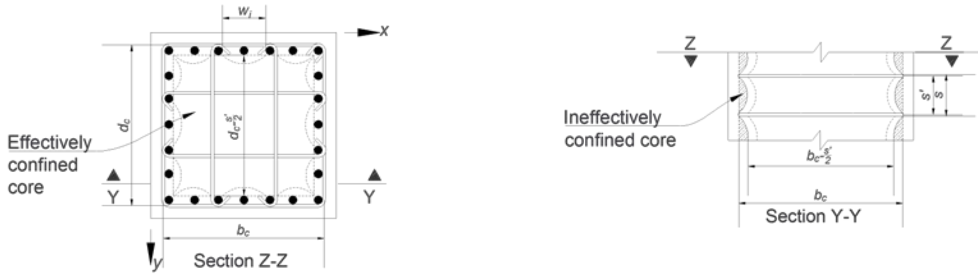

Fig. 3 – Geometrical parameters of Mander model for confined concrete [9]

Lateral confining pressure is assumed to be uniformly distributed over concrete surface; in *x* and *y* direction, it is given by $\sigma_{\mathrm{lx}} = \rho_{\mathrm{x}} f_{\mathrm{yh}}$ and $\sigma_{\mathrm{ly}} = \rho_{\mathrm{y}} f_{\mathrm{yh}}$, respectively. In these expressions, ρ_x and ρ_y refer to transverse reinforcement amounts in *x* and *y* direction (Fig. 3), respectively. Noticeably, ρ_x and ρ_y include hoops and ties. f_{yh} is yield point of transverse reinforcement.

Since this model can experience numerical instabilities under large displacements, the modifications suggested by [10] are considered; the therefrom-arising model can predict the strength and stiffness degradation under cyclic motion. Tensile concrete strength is neglected. The behavior of the reinforcement steel is described by uniaxial bilinear constitutive laws with 4‰ kinematic strain hardening; the hardening rule for the yield surface is a linear function of the increment of plastic strain.

2.5 Numerical model of pounding

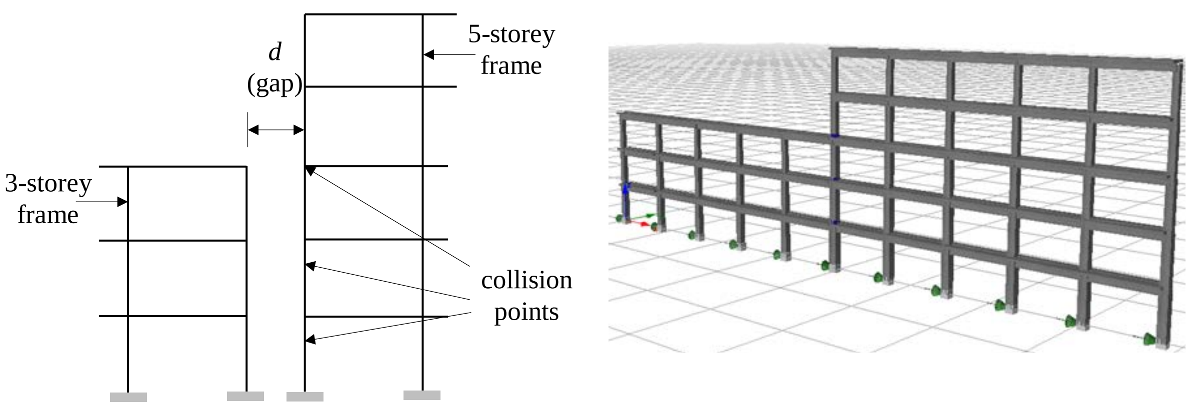

(a) Sketch of the frames (b) Numerical model of the frames

Fig. 4 – Considered pounding frames

The prototype buildings are assumed to collide by pairs. As an example, Fig. 4 describes pounding between 3 × 5 and 5 × 5 buildings. Fig. 4.a shows a detail of two colliding frames and Fig. 4.b displays a 3D global representation of such frames; this last image has been taken from the numerical model considered in the analysis. The gap indicated in Fig. 4.a represents the initial separation between the frames; the considered values of the gap size (*d*) are 0, 2 and 4 cm. Noticeably, for 4 cm there is no pounding in virtually all the situations.

The pounding effect is described with linear Kelvin-Voigt gap models (parallel combination of a spring and a dashpot) located in each story. Fig. 5 displays the considered model. In Fig. 5, *d* is the gap size, *x* represents the sum of shortenings of both colliding slabs, *k* is the spring stiffness and *c* is the dashpot damping. Coefficient *c* is related to damping factor ζ by

$$c = 2\,\zeta \sqrt{k\,\frac{m_1 m_2}{m_1 + m_2}} \tag{3}$$

In Eq. (3) masses m_1 and m_2 correspond to the colliding bodies; more precisely, m_1 and m_2 represent the lumped masses for each model of the pounding buildings. Despite this model is termed as linear, it is actually nonlinear, since gap behaves as a "compression only" element.

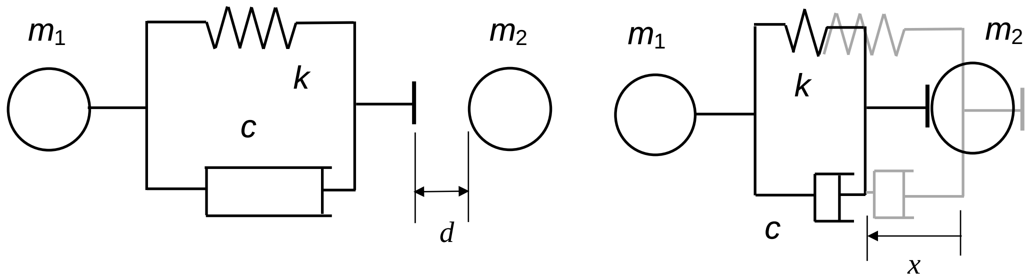

(a) Model in undeformed configuration (b) Model in deformed configuration

Fig. 5 – Linear Kelvin-Voigt gap model of pounding

Constitutive law is given by equation

$$\begin{aligned} f &= k\,x + c\,\dot{x} \qquad &\text{if} \quad x - d \geq 0 \\ f &= 0 \qquad &\text{if} \quad x - d < 0 \end{aligned} \tag{4}$$

The stiffness (k) of the spring is selected proportional to the axial stiffness of the colliding slabs as $k = \alpha\,(E\,A\,/\,L)$ (Fig. 5) where E, A and L are moduli of elasticity (concrete), cross-section areas and lengths of colliding slabs, which E, A and L belong to the longest colliding slab. α is a stiffness coefficient ($\alpha > 1$) [12] that accounts for the higher influence of the slab segments that are closer to the impact point. The damping factor is chosen as to provide a desired restitution factor (r) as [13]

$$\zeta = -\ln r \,/\, (\pi^2 + \ln^2 r)^{1/2} \tag{5}$$

In Eq. (5), two values of the restitution factor are considered: 0.527 and 0.729 [14]; the corresponding values of the damping factor are 0.1 and 0.2, respectively.

3. Seismic inputs

Four representative inputs are selected; are obtained combining the presence or absence of velocity pulses and stiff / soft soil conditions. Table 4 depicts the most relevant characteristics of the four chosen representative inputs [15]. I_A is the Arias Intensity [16] given by $I_A = \frac{\pi}{2\,g} \int \ddot{x}_g^2 \, dt$ where $\ddot{x}_g$ is the input ground acceleration; the Arias intensity is an estimator of the input severity. I_D is the dimensionless seismic index [17] given by $I_D = \frac{\int \ddot{x}_g^2 \, dt}{PGA\;PGV}$. The dimensionless index accounts broadly for the velocity pulses content; small/big values of I_D correspond to records with/without pulses. PI is the pulse index [18], which takes values between 0 and 1; records with scores above 0.85 and below 0.15 are classified as pulses and non-pulses, respectively. E_p is the relative pulse energy [19], representing the portion of the total energy of the ground motion that corresponds to the pulse. The pulse is extracted by the peak-point method [20]. Values of E_p greater than 0.3 correspond to pulse-like records and values equal to or below 0.3 are ambiguous. The Trifunac duration is defined as the time between the 5% and the 95% of the Arias Intensity I_A [21]. The hypocentral distance corresponds to the straight separation between the hypocenter and the recording station. The closest distance corresponds to the shortest way to the rupture surface [15]. v_{s30} is the average shear wave velocity in the top 30 m. The soil type in the last column corresponds to the classification of the Eurocode 8 [4].

Table 4 – Considered input records

Earthquake	Date	M_w	Hypo-center depth [km]	Station	Comp.	PGA [g]	PGV [m/s]	I_A [m/s]	I_D	*PI*	E_p	Trifunac duration [s]	Hypo-central distance [km]	Closest distance ClsD [km]	V_{s30} [m/s]	Soil type (EC8)	Name
Northridge	1994	6.7	17.5	Sylmar-Olive	CDMG24514	0.843	1.295	5.01	2.92	1.0	0.61	5.32	24.24	5.3	440.5	B	P B
Northridge	1994	6.7	17.5	W Pico Canyon	UCS90056	0.455	0.927	1.54	2.33	1.0	0.70	6.59	27.76	5.48	285.9	C	P C
Victoria Mexico	1980	6.3	11	Cerro Prieto	UCSD6604	0.62	0.316	1.97	6.38	0.0025	0.14	8.57	35.48	14.37	659.6	B	NP B
Northridge	1994	6.7	17.5	Saticoy St	USC90003	0.48	0.615	4.6	9.98	5.07×10^{-4}	0.34	10.61	17.83	12.09	280.9	C	NP C

Observing values of *PI* and E_p, Table 4 shows clearly that first two inputs (Northridge Sylmar-Olive and W Pico Canyon) are Pulse-like and that last two inputs (Victoria Cerro Prieto and Northridge Saticoy St) are not Pulse-like. Next in this work, four inputs listed in Table 4 are termed P B, P C, NP B and NP C, respectively. In this notation, "P" and "NP" account for Pulse and Non-Pulse, respectively, and "B" and "C" refer to soil type. To highlight the major characteristics of the four selected ground motion records, Fig. 6 displays their time histories.

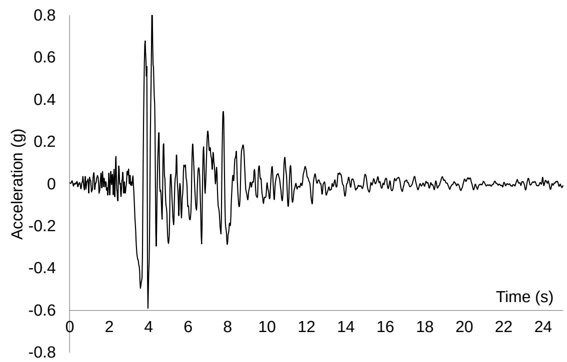

(a) Northridge Sylmar-Olive (P B)

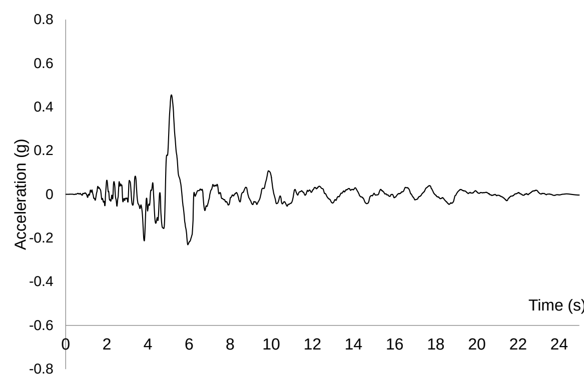

(b) Northridge W Pico Canyon (P C)

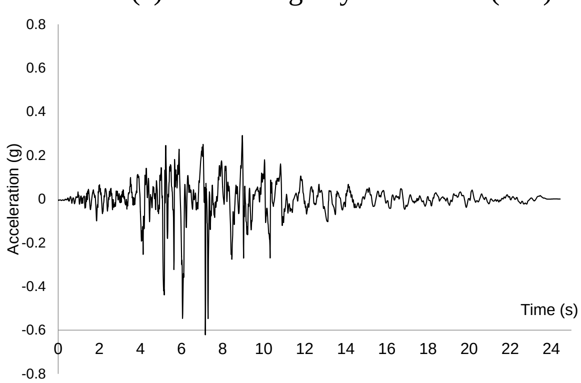

(c) Victoria Cerro Prieto (NP B)

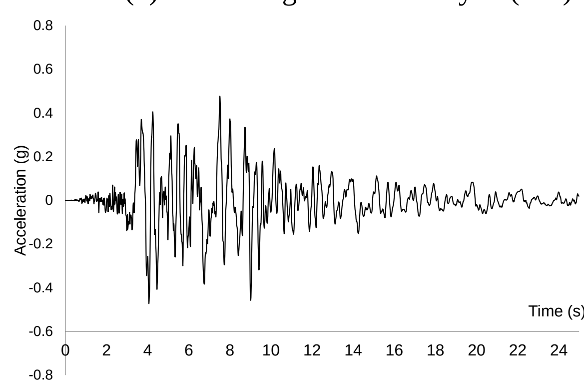

(d) Northridge Saticoy St (NP C)

Fig. 6 – Considered input accelerograms

Observation of accelerograms displayed in Fig. 6 confirms that those in top plots are obviously Pulse-like, while those in bottom plots are not. As well, left plots exhibit higher high-frequency contents than those in right plots, this being coherent with soil type.

4. Parametric study

4.1 Parameters of the study

A number of nonlinear dynamic analyses are carried out to investigate the pounding behavior of the prototype buildings. The parameters of the study are:

- **Buildings**. The four representative prototype buildings are described in section 2.
- **Input**. The four seismic inputs are described in section 3.
- **Impact model**. The impact model is described in subsection 2.5. It is characterized by three major parameters: stiffness coefficient (α), damping ratio (ζ) and gap size (d).
- **SSI analysis**. Soil-Structure Interaction.

Table 5 displays the cases that are analyzed.

Table 5 – Parameters of the performed analyses

Buildings	**Input**		**Impact model**			**SSI**	**Notation**	**No.**
	Near-fault effects	**Soil type**	α	ζ	***d*** **(cm)**			
3 × 5 | 5 × 2	Pulse	C	2	0.1	2	NO	P C / 2 / 0.1 / 2	1
	Pulse	C	5	0.1	2	NO	P C / 5 / 0.1 / 2	2
						ISOL.		3
						MAT		4
	Pulse	C	10	0.1	2	NO	P C / 10 / 0.1 / 2	5
	Non Pulse	B	5	0.1	2	NO	NP B / 5 / 0.1 / 2	6
	Non Pulse	C	5	0.1	2	NO	NP C / 5 / 0.1 / 2	7
						ISOL.		8
						MAT		9
5 × 5 | 5 × 2	Pulse	C	5	0.1	0	NO	P C / 5 / 0.1 / 0	10
						ISOL.		11
						MAT		12
	(+) Non Pulse(*)	B	5	0.1	0	NO	NP+ B / 5 / 0.1 / 0	13
	(–) Non Pulse(*)	B	5	0.1	0	NO	NP– B / 5 / 0.1 / 0	14
	Non Pulse	C	5	0.1	4	NO	NP C / 5 / 0.1 / 4	15
	Non Pulse	C	5	0.1	2	NO	NP C / 5 / 0.1 / 2	16
						ISOL.		17
						MAT		18
	Non Pulse	C	5	0.1	0	NO	NP C / 5 / 0.1 / 0	19
						ISOL.		20
						MAT		21
5 × 5 | 3 × 2	(+) Pulse(*)	B	5	0.1	2	NO	P+ B / 5 / 0.1 / 2	22
	(–) Pulse(*)	C	5	0.1	2	NO	P– C / 5 / 0.1 / 2	23
						ISOL.		24
						MAT		25
	Non Pulse	C	2	0.1	2	NO	NP C / 2 / 0.1 / 2	26
	Non Pulse	C	5	0.1	2	NO	NP C / 5 / 0.1 / 2	27
						ISOL.		28
						MAT		29
	Non Pulse	C	5	0.1	0	ISOL.	NP C / 5 / 0.1 / 0	30
	Non Pulse	C	10	0.1	2	NO	NP C / 10 / 0.1 / 2	31
5 × 2 | 3 × 2	Pulse	B	5	0.1	2	NO	P B / 5 / 0.1 / 2	32
	Non Pulse	C	2	0.1	2	NO	NP C / 2 / 0.1 / 2	33
	Non Pulse	C	2	0.2	2	NO	NP C / 2 / 0.2 / 2	34
	Non Pulse	C	5	0.1	2	NO	NP C / 5 / 0.1 / 2	35
						ISOL.		36
						MAT		37
	Non Pulse	C	10	0.1	2	NO	NP C / 10 / 0.1 / 2	38

(*) ± indicates that the input is either multiplied by + 1 or by – 1; this represents opposite orientations of the colliding buildings

4.2 Performance indices

Since the major objective of this research is to investigate the consequences of seismic pounding between adjoining buildings with aligned slabs, it is crucial to establish a number of criteria (performance indices) for appraising each case. These indices are intended to summarize, in a quantifiable way, the major results of the dynamic analyses. Four evaluation magnitudes are selected:

- **Maximum drift angle**. Ratio between inter-story drift displacement and story height. This value provides, for each story, information on the damage on the structural members (beams and columns) and infill walls.
- **Maximum shear force**. Reports, as drift, on the structural damage at each story. Shear force is directly correlated to risk of brittle shear failure of columns. In the first floor, the shear force is the base shear force; it provides information on the demanding forces on the foundation.
- **Hysteretic energy**. Absorbed energy minus the energy absorbed by the initial damping of the structure; therefore is the damaging part of input energy. This energy is also termed as "contributable to damage". Reports on the structural damage in terms of cumulated values (plastic excursions).
- **Maximum absolute acceleration**. Provides information on the damage to the non-structural components (non-structural damage). This quantity is correlated to risk of debris fall and other similar effects, such as out-of-plane failure of infill walls.

Noticeably, all these indices can be determined for each story. Moreover, the addition of the hysteretic energy for all the stories yields the energy for the whole building.

Beyond the above major indices, other magnitudes that are directly related to impact might provide, under certain circumstances, relevant information. Among them: maximum value of the contact force, impact duration, and relative velocity at impact. These quantities report on the severity of impact, being correlated with the difference between cases with and without pounding.

4.3 Results

This subsection presents preliminary results of the dynamic analyses corresponding to case No. 7 (Table 5). Results are presented in terms of the evaluation quantities (performance indices) described in subsection 4.2. Fig. 7 displays, for each story, major outputs for one pair of colliding buildings (Table 1) under the selected inputs (Table 4). Black/grey plots correspond to cases with/without pounding, respectively. Fig. 7.a and Fig. 7.b represent the maximum drift angles. Fig. 7.c and Fig. 7.d display the maximum story shear force. Fig. 7.e and Fig. 7.f show the hysteretic energy. Fig. 7.g and Fig. 7.h show the maximum absolute accelerations. Plots for the left / right buildings are displayed on left / right Figures (#.a, #.c, #.e, #.g / #.b, #.d, #.f, #.h), respectively.

In Fig. 7.a and Fig. 7.b, positive sign corresponds to clockwise angle, i.e. the right displacement of the above story is bigger ( ). In Fig. 7.c and Fig. 7.d, positive sign corresponds to forces generating positive shear strains ( ), as in Fig. 7.a and Fig. 7.b. In Fig. 7.g and Fig. 7.h, positive sign corresponds to outward acceleration, i.e. elements are pushed to fall inward ( ).

Noticeably, in Fig. 7.a, Fig. 7b, Fig. 7.c, Fig. 7.d, Fig. 7.g and Fig. 7.h, the maximum values for each story are not necessarily simultaneous; this means that the plotted profiles do not represent the situation of the structures in any instant. Due to this fact, the interpretations become more difficult.

Plots from Fig. 7 allow deriving the following preliminary remarks:

- In the top stories (those above the colliding third floor) of the taller buildings (5 × 2), energy is increased, and drift is also increased in inward direction. Both effects are generated by the inward slash motion of the top two protruding stories of the taller building after receiving the impact of the shorter building.
- Acceleration is increased, in the pounding story, in outward direction. This effect is due to after-impact bounce.

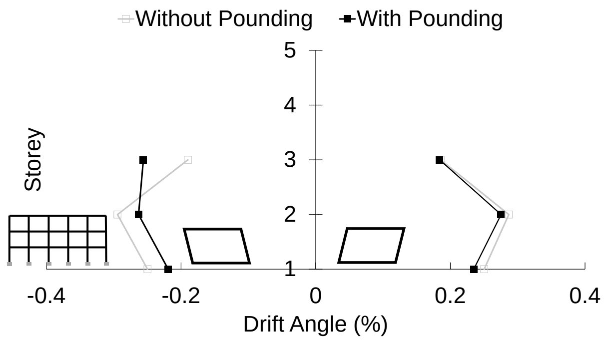

(a) Maximum drift angle in the 3 × 5 building (left)

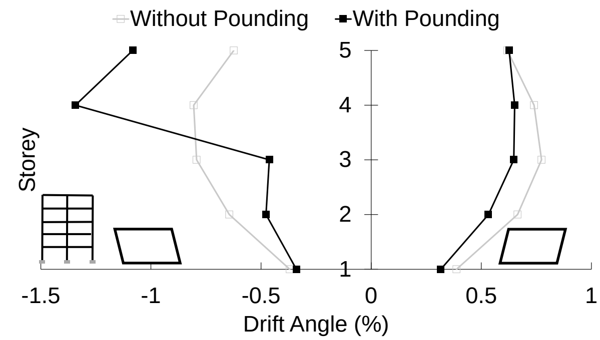

(b) Maximum drift angle in the 5 × 2 building (right)

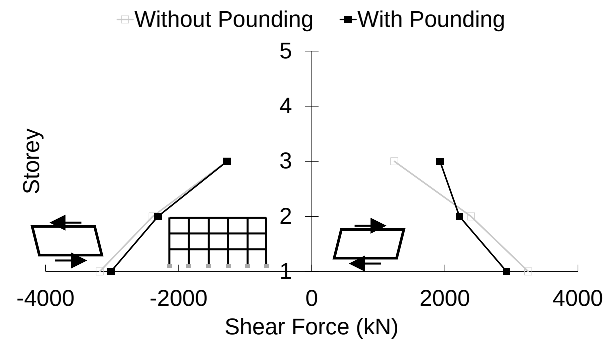

(c) Maximum story shear force in the 3 × 5 building (left)

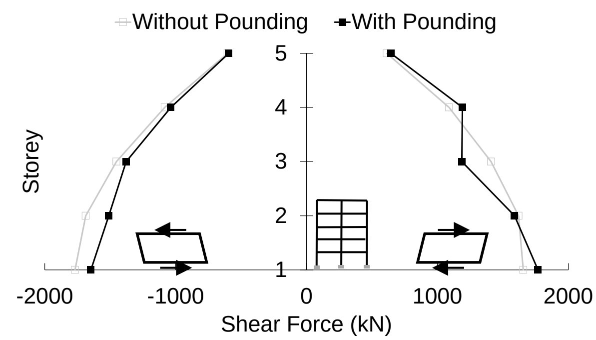

(d) Maximum story shear force in the 5 × 2 building (right)

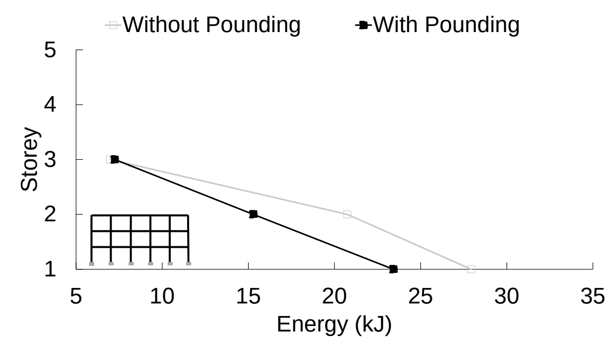

(e) Hysteretic energy in the 3 × 5 building (left)

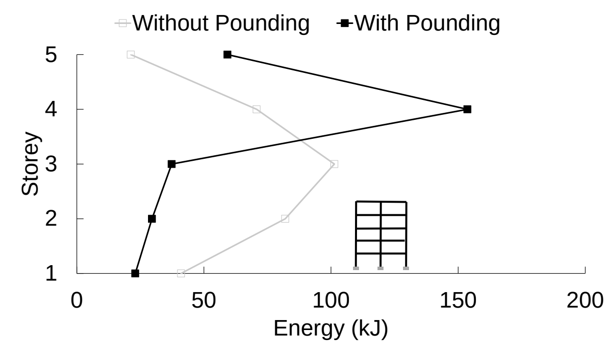

(f) Hysteretic energy in the 5 × 2 building (right)

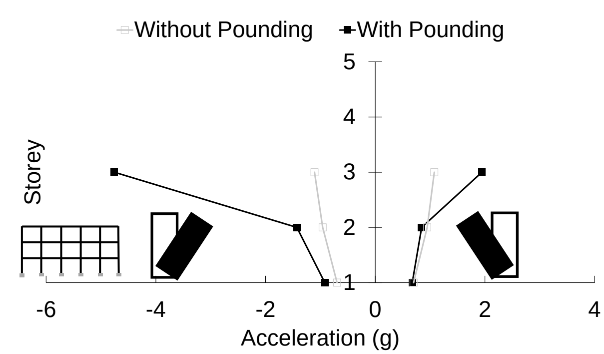

(g) Maximum absolute acceleration in the 3 × 5 building (left)

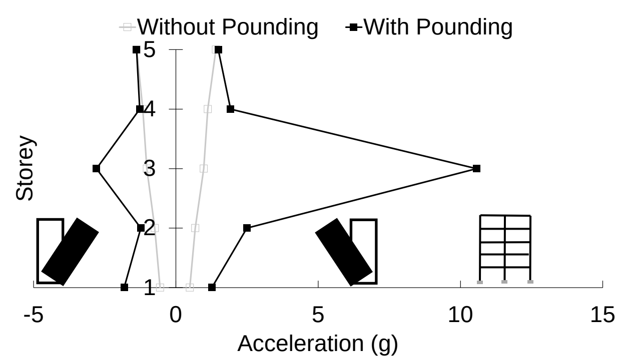

(h) Maximum absolute acceleration in the 5 × 2 building (right)

Fig. 7 – Responses with / without pounding. 3 × 5 | 5 × 2; k = 2246 kN/mm (α = 5); ζ = 0.1 (r = 0.729); d = 2 cm. Northridge Saticoy St. (NP C) (Table 4)

5. Conclusions

These preliminary results show regular and expected behavior. This validates accuracy and reliability of the used model. Further research is currently in progress; a new formulation for estimating the parameters is developed.

6. Acknowledgements

This work has received financial support from Spanish Government under projects BIA2014-60093-R and CGL2015-6591. These supports are gratefully acknowledged.

7. References

[1] Kasai K, Maison BF (1997): Building pounding damage during the 1989 Loma Prieta earthquake, *Engineering Structures*, **19** (3), 195–297.

[2] ACI-318-11 (2011): *Building Code Requirements for Structural Concrete*, American Concrete Institute.

[3] ASCE/SEI 7-10 (2010): *Minimum Design Loads for Buildings and other Structures*. American Society of Civil Engineers.

[4] EN-1998 (2004): *Eurocode 8: Design of structures for earthquake resistance*, European Committee for Standardization.

[5] FEMA 356 (2000): *Prestandard and Commentary for the Seismic Rehabilitation of Buildings*, Federal Emergency Management Agency (FEMA).

[6] Seismosoft (2015): SeismoStruct v7.06 – *A computer program for static and dynamic nonlinear analysis of framed structures*, Package for processing of strong-motion data available from http://www.seismosoft.com.

[7] Scott MH, Fenves GL (2006): Plastic hinge integration method for force-based beam-column elements, *Journal of Structural Engineering*, **132** (2), 244-252.

[8] Paulay T, Priestly MJN (1992): *Seismic Design of Reinforced Concrete and Masonry Buildings*, John Wiley.

[9] Mander JB, Priestley MJN, Park R (1988): Theoretical stress-strain model for confined concrete, *Journal of Structural Engineering*, **114** (8), 1804-1826.

[10] Martínez-Rueda JE, Elnashai AS (1997): Confined concrete model under cyclic load, *Materials and Structures*, **30** (197), 139-147.

[11] Madas P (1993): *Advanced Modelling of Composite Frames Subjected to Earthquake Loading*, PhD Thesis, Imperial College, London, UK.

[12] Muthukumar S, DesRoches R (2006): A Hertz contact model with non-linear damping for pounding simulation, *Earthquake Engineering & Structural Dynamics*, **35**, 811–828.

[13] Anagnostopoulos SA (2004): Equivalent viscous damping for modelling inelastic impacts in earthquake pounding problems, *Earthquake Engineering & Structural Dynamics*, **33** (8), 897-902.

[14] Anagnostopoulos SA, Spiliopoulos KV (1992): An investigation of earthquake induced pounding between adjacent buildings, *Earthquake Engineering and Structural Dynamics*, **21** (4), 289–302.

[15] PEER Ground Motion Database. http://peer.berkeley.edu/products/strong_ground_motion_db.html.

[16] Arias A (1970): A measure of earthquake intensity. Seismic Design for Nuclear Power Plants, MIT Press 438-443.

[17] Manfredi G (2001): Evaluation of Seismic Energy Demand, *Earthquake Eng. & Structural Dynamics*, **30**, 485–499.

[18] Baker JW (2007): Quantitative Classification of Near-Fault Ground Motions Using Wavelet Analysis, *Bulletin of the Seismological Society of America*, **97** (5),1486–1501.

[19] Zhai C, Chang Z, Li S, Chen Z, Xie L (2013): Quantitative Identification of Near-Fault Pulse-Like Ground Motions Based on Energy, *Bulletin of the Seismological Society of America*, **103** (5), 2591–2603.

[20] Dickinson BW, Gavin HP (2011): Parametric statistical generalization of uniform-hazard earthquake ground motions, *Journal of Structural Engineering*, **137** (3), 410-422.

[21] Trifunac MD, Brady AG (1975): Study on the duration of strong earthquake ground motion, *Bulletin of the Seismological Society of America*, **65** (3):581–626.